

Biorenewable, transparent, and oxygen/moisture barrier nanocellulose/nanochitin-based coating on polypropylene for food packaging applications

Hoang-Linh Nguyen^{a,b,1}, Thang Hong Tran^{a,c}, Lam Tan Hao^{a,c}, Hyeonyeol Jeon^a, Jun Mo Koo^a, Giyoung Shin^a, Dong Soo Hwang^{b,*}, Sung Yeon Hwang^{a,c,*}, Jeyoung Park^{a,c,*}, Dongyeop X. Oh^{a,c,*}

^a Research Center for Bio-based Chemistry, Korea Research Institute of Chemical Technology (KRICT), Ulsan 44429, Republic of Korea

^b Division of Environmental Science & Engineering, Pohang University of Science and Technology (POSTECH), Pohang 37673, Republic of Korea

^c Advanced Materials and Chemical Engineering, University of Science and Technology (UST), Daejeon 34113, Republic of Korea

ARTICLE INFO

Keywords:

Cellulose nanofiber
Chitin nanowhisker
Polypropylene
Layer-by-layer assembly
Dip coating
Food packaging

ABSTRACT

Aluminum-coated polypropylene films are commonly used in food packaging because aluminum is a great gas barrier. However, recycling these films is not economically feasible. In addition, their end-of-life incineration generates harmful alumina-based particulate matter. In this study, coating layers with excellent gas-barrier properties are assembled on polypropylene films through layer-by-layer (LbL) deposition of biorenewable nanocellulose and nanochitin. The coating layers significantly reduce the transmission of oxygen and water vapors, two unfavorable gases for food packaging, through polypropylene films. The oxygen transmission rate of a 60 μm -thick, 20 LbL-coated polypropylene film decreases by approximately a hundredfold, from 1118 to 13.10 $\text{cc m}^{-2} \text{day}^{-1}$ owing to the high crystallinity of nanocellulose and nanochitin. Its water vapor transmission rate slightly reduces from 2.43 to 2.13 $\text{g m}^{-2} \text{day}^{-1}$. Furthermore, the coated film is highly transparent, unfavorable to bacterial adhesion and thermally recyclable, thus promising for advanced food packaging applications.

1. Introduction

Food packaging materials are vital components in daily life (Garavand et al., 2017; Garavand et al., 2020; Lange & Wyser, 2003; Marsh & Bugusu, 2007). The global market revenue of plastic packaging materials totaled USD 375.0 billion in 2020 and is forecasted to reach USD 486.2 billion by 2028 (Grand View Research Inc., 2020). Packages protect foods from biochemical and mechanical damage. Another appealing function is their high transparency, which provides customers with a clear visibility of the content inside (Lange & Wyser, 2003; Jinwu Wang et al., 2018).

Food packaging also needs to possess barrier properties which prevent premature food spoilage by factors such as oxygen gas and water vapor. For decades, the scientific community has devoted significant effort to finding high-performance gas-barrier materials. For example, halogenated polymers such as poly(vinylidene chloride) (PVDC) are an excellent gas-barrier coating layer for plastic films, but their end-use combustion generates hazardous gases that heavily pollute the

environment (Lange & Wyser, 2003; Jinwu Wang et al., 2018). Inorganic nanomaterials such as nanoclays and layered double hydroxides can be used to construct a high gas barrier (Priolo et al., 2010; Yu et al., 2019). However, adverse human health effects related to inorganic nanoparticle exposure have been well documented (Boyes & Van Thriel, 2020). All-polymer films with low oxygen permeability were fabricated from synthetic polyethylenimine and poly(acrylic acid), but their crosslinking involved cytotoxic glutaraldehyde (Yang et al., 2011). These limitations necessitate the development of next-generation high-performance barrier materials which can integrate multifunctionalities of being transparent, renewable, biofriendly, and easily recyclable for food packaging applications (Kim et al., 2019; Kiryukhin et al., 2018).

Cellulose and chitin are the two most abundant biorenewable resources. They have received attention from research and industry owing to their comprehensive properties (strength, transparency, biocompatibility, and biodegradability) and the public increasing demand for sustainable development (Kim et al., 2019; Reid et al., 2017; Yan & Chen, 2015). Cellulose and chitin are mainly found in higher plants and

* Corresponding authors at: Research Center for Bio-based Chemistry, Korea Research Institute of Chemical Technology (KRICT), Ulsan 44429, Republic of Korea. E-mail addresses: dshwang@postech.ac.kr (D.S. Hwang), crew75@kRICT.re.kr (S.Y. Hwang), jypark@kRICT.re.kr (J. Park), dongyeop@kRICT.re.kr (D.X. Oh).

¹ Deceased August 28th, 2020

<https://doi.org/10.1016/j.carbpol.2021.118421>

Received 11 March 2021; Received in revised form 20 June 2021; Accepted 6 July 2021

Available online 10 July 2021

0144-8617/© 2021 The Author(s).

Published by Elsevier Ltd.

This is an open access article under the CC BY-NC-ND license

(<http://creativecommons.org/licenses/by-nc-nd/4.0/>).

crustaceans, respectively, where they self-assemble into hierarchically ordered nano-/macro- structures (Cacciotti et al., 2014; Nikolov et al., 2010; Zimmermann et al., 2004). Various top-down methods can transform bulk cellulose and chitin into nanomaterials with high crystallinity (Reid et al., 2017; Zhang & Rolandi, 2017), which is a desirable feature for gas-barrier materials. Furthermore, appropriate surface modification can introduce functional groups on cellulose/chitin-derived nanomaterials and improve their aqueous processability (Iso-gai et al., 2011; T. H. Tran et al., 2019), providing more opportunity for industrial scale-up.

A gas barrier can be constructed on a plastic substrate surface through layer-by-layer (LbL) assembly of oppositely charged components (Decher & Hong, 1991; Priolo et al., 2015; Richardson et al., 2015; Richardson et al., 2016; Yang et al., 2011). Due to its flexibility and robust control of coating layers, LbL assembly has found applications in various fields including desalination (Abbaszadeh et al., 2019; Halakoo & Feng, 2020), microalgae harvesting (Huang et al., 2020), waste treatment (Luo et al., 2020; Jingyu Wang et al., 2020), flame retardant (X. Liu et al., 2020; Qiu et al., 2019), heavy metal removal (Hosseini et al., 2020), drug delivery (Kalaycioglu & Aydogan, 2020), wearable electronic devices (Oytun & Basarir, 2019), sensors (Ni et al., 2019), biocide delivery (Cai et al., 2019), supercapacitors (Tian et al., 2019), wound dressing and healing (Richardson et al., 2016), and gas barrier (Heo et al., 2019).

We previously showed that an LbL assembly of positively charged nanochitin and negatively charged nanocellulose on poly(ethylene terephthalate) (PET) films afforded a high oxygen barrier required for the food packaging application because the two nanomaterials complement each other well, driven by their strong electrostatic attraction (Kim et al., 2019). However, their high moisture permeability remains unsolved as a universal problem for hydrophilic materials (Jinwu Wang et al., 2018). To this end, polypropylene (PP), the most used commodity plastic in the food industry, represents a great moisture-barrier material (Lange & Wyser, 2003; Marsh & Bugusu, 2007; Michiels et al., 2017). PP films are also safe for human use when applied as rolled grocery bags (Maier & Calafut, 1998). However, the critical limitation of PP films is their high oxygen permeability. A 30–60 μm -thick PP film exhibits a low water vapor transmission rate (WVTR) of $<10 \text{ cc m}^{-2} \text{ day}^{-1}$ but a high

oxygen transmission rate (OTR) of $800\text{--}1700 \text{ cc m}^{-2} \text{ day}^{-1}$ (Lange & Wyser, 2003; Nakaya et al., 2015).

If the weak oxygen barrier of PP films can be solved with a simple method, they can become a robust food packaging material. Aluminum metalization is considered a standardized method to produce a high oxygen barrier (Struller et al., 2014) but at the expense of losing transparency and recyclability of coated films. Several recent studies have enabled the preparation of a high gas-barrier coating layer, replacing aluminum, onto PP (d'Eon et al., 2017; P. Lu et al., 2018; Ozcalik & Tihminlioglu, 2013; Song et al., 2016). Nevertheless, they involved either non-renewable materials or methods that are complex to reproduce, automate and scale up. In some cases, the OTR of coated PP films could not be significantly reduced to meet the packaging requirement for certain types of food such as fresh meat, grains and nuts.

In this study, we demonstrated that LbL assembly of biorenewable nanomaterials, which was successfully applied to PET, can be expanded to produce high-performance gas barrier-coated PP films. Multiple LbL of oxygen-proof negatively charged cellulose nanofibers and positively charged chitin nanowhiskers were constructed on a moisture-proof PP film, producing a high dual barrier-coated film through a simple immersive coating technique (Fig. 1). Dimensions, surface features, colloidal stability, and chemical and crystal structures of the two nanomaterials were confirmed prior to coating. Film structures were analyzed with attenuated total reflection Fourier-transform infrared spectroscopy (ATR-FTR), field-emission scanning electron microscopy (FE-SEM), contact angle measurement, and UV-vis spectroscopy. Effects of coating layers on the barrier performance against oxygen and water vapors of PP films were investigated. In addition, coated PP films were tested for their mechanical, antibacterial and thermal properties.

2. Experimental

2.1. Reagents and culture media

Biaxially oriented polypropylene films and aluminum-metalized PP films were provided by SK Chemicals (South Korea). Shrimp shells-derived, bulk α -chitin (practical grade), NaOH pellets (97%), H_2SO_4 solution (95–98%) were purchased from Sigma-Aldrich (USA).

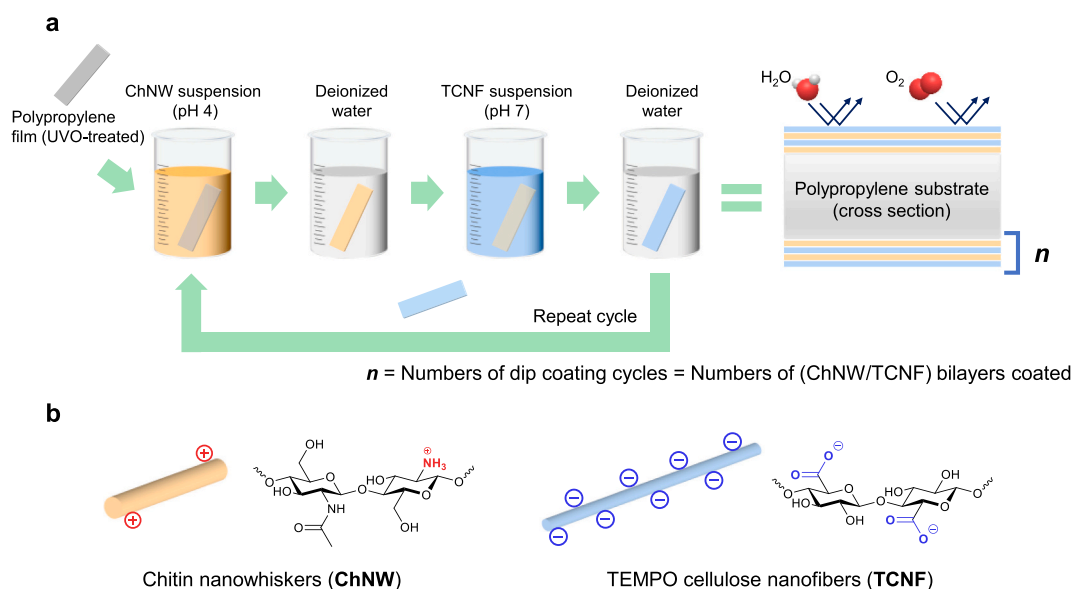


Fig. 1. (a) Schematic illustration of layer-by-layer (LbL) assembly of chitin nanowhiskers (ChNW) and TEMPO cellulose nanofibers (TCNF) through dip coating onto polypropylene (PP) films, pre-irradiated with ultraviolet/ozone (UVO). One dip coating cycle affords one (ChNW/TCNF) bilayer, which is denoted as n . Concentrations of coating suspensions are 0.2, 0.4, and 0.8 wt% for TCNF, and 0.8, 1.6, 2.4, and 3.2 wt% for ChNW. The coated PP film exhibits high barrier properties against oxygen gas and water vapor for food packaging application. (b) Chemical structures of ChNW and TCNF and a relative comparison in terms of dimension and surface charge (type and density) between the two nanomaterials.

Concentrated HCl solution (35 wt%) and H₂O₂ solution (30 wt%) were purchased from Daejung (S. Korea). Difco LB Broth, Miller (Luria-Bertani, pH 7.0 ± 0.2) was obtained from BD Biosciences (USA). All materials were stored as providers' instructions and used as received without further purification.

Deionized water was purified from tap water using a water purification system (Milli-Q Integral 3, Millipore, USA) and has a final resistivity of 18.0 MΩ cm at 25 °C.

2.2. Nanomaterials

TEMPO cellulose nanofibers (TCNF) were purchased from US Department of Agriculture (USDA) Forest Products Laboratory through University of Maine as freeze-dried powder. TCNF was produced by treating pulp with TEMPO [(2,2,6,6-tetramethyl piperidine-1-yl)oxyl radical]-mediated oxidation process, co-catalyzed by NaClO and NaBr as previously reported (Ferrer et al., 2017; Isogai et al., 2011; Saito et al., 2007). TEMPO selectively oxidizes primary hydroxyl groups of cellulose (C6-OH) to carboxylic acid, whereas NaClO and NaBr are used to re-oxidize TEMPO for further reaction.

Chitin nanowhiskers (ChNW) were fabricated in our laboratory through glycosidic hydrolysis of amorphous regions of shrimp shells-derived α-chitin using hydrochloric acid (Yongwang Liu et al., 2018; Marchessault et al., 1959; Revol & Marchessault, 1993; T. H. Tran et al., 2019). Briefly, α-chitin (10 g) was suspended in HCl (3 M, 300 mL) and refluxed at 120 °C for 3 h. After the reaction, the suspension was repeatedly diluted, washed with deionized water, and centrifuged (5000 rpm, 20 min, 10 °C) using a high-speed centrifuge (Supra 30R, Hanil, S. Korea) until the supernatant become turbid. The ChNW pellets were resuspended, dialyzed against deionized water using dialysis tubing with a molecular weight cut-off of 10 kDa (Spectrum Labs Spectra/Por 6, Fisher Scientific, USA) for several days. The dialysis process was monitored through the conductivity of the dialysate until salts and hydrolyzed byproducts were removed. The dialyzed suspension was ultrasonicated in a water-cooling bath using a cell disruptor (Sonics VCX-750-220, USA) at 40% amplitude (5 s/2 s-on/off cycles) for several minutes until ChNW became well dispersed (indicated by a homogenous translucency). Finally, the suspension was freeze-dried at -50 °C using a freeze dryer (IlshinBiobase FD8512, S. Korea) for one week.

For PP coating and subsequent analyses, freeze-dried ChNW and spray-dried TCNF were redispersed in deionized water by ultrasonication. The pH of resulting suspensions was adjusted to 4 for ChNW and 7 for TCNF using HCl or NaOH solution (0.01 M). The pH adjustment creates charges on nanomaterial surfaces that colloiddally stabilize the suspensions through repulsive forces (Kim et al., 2019).

2.3. Layer-by-layer coating of polypropylene films

PP substrates were cleaned with deionized water and methanol and then irradiated with ultraviolet/ozone (UVO) for 20 min using a UV-ozone cleaner (AHTech AC-6, S. Korea) to improve hydrophilicity and surface adhesion (Allahvaisi, 2012; MacManus et al., 1999; Walzak et al., 1995; Y. Wang et al., 2000). The suspension concentrations were varied for TCNF (0.2, 0.4, and 0.8 wt%) and ChNW (0.8, 1.6, 2.4, and 3.2 wt%) to optimize the barrier performance of the coating layers (Supporting Information). UVO-treated PP substrates were alternately immersed in a ChNW suspension for 3 min (the first coating layer), rinsed with deionized water, immersed in a TCNF suspension for 3 min, and rinsed again with deionized water. One complete dip coating cycle afforded one bilayer of ChNW/TCNF and was repeated until a desired number (*n*) of (ChNW/TCNF)-bilayers were obtained (Fig. 1a). Coated films were dried at 80 °C for one day to remove remaining moisture prior to further characterization.

2.4. Characterization

2.4.1. Field-emission scanning electron microscopy

Dry silicon wafers (QL Electronics, China) are of p-type (boron-doped), single-sided-polished and have an average thickness of 525 ± 25 μm and a resistivity of <0.005 Ω. The wafers were first immersed in a piranha solution (H₂SO₄: H₂O₂ 7:3 v/v) to etch organic residues and make the surface highly hydrophilic. *Caution: Piranha solution is a strong oxidizing agent and strongly acidic, therefore should be handled with great care using appropriate protection.* Next, cleaned wafers were rinsed with deionized water and acetone and dried under ambient conditions before use.

Serial tenfold dilutions of 0.1 wt% aqueous suspensions of TCNF and ChNW were made, and 30 μL of the 10⁻⁴-diluted suspension was dropped on the polished side of a clean wafer (1 cm × 1 cm). The wafer was dried *in vacuo* at 80 °C for 24 h prior to SEM. PP samples were fixed to a clean wafer using a double-sided carbon tape to observe their cross sections. An FE-SEM (Tescan MIRA3, Czech Republic) with a secondary electron detector was employed to observe the morphology of nanomaterials and PP films. The wafers were coated with a Pt layer at 15 mA for 90 s using a turbomolecular pumped coater (Quorum Technologies Ltd. Q150 T Plus, UK) before SEM observation.

Size measurements of nanomaterials were done on 50 random individualized fibers/whiskers by processing the SEM images of nanomaterials using ImageJ program v. 1.5.8 (National Health Institute, USA).

2.4.2. Surface zeta potential

The surface zeta potentials (ζ-potentials) which are related to surface charge and colloidal stability of TCNF and ChNW were measured using a Zetasizer Nano ZS device (Malvern, UK) equipped with a folded capillary zeta cell (DTS1070). Aqueous TCNF and ChNW suspensions were prepared at 0.001 wt%, and pH adjustment defines the double-layer thickness around the nanomaterials so that accurate zeta potential values could be obtained (Yongwang Liu et al., 2018; Reid et al., 2017). Each measurement was done at 25 °C and composed of 100 cycles to obtain an average value.

2.4.3. Surface functional group content

The surface functional group contents of TCNF and ChNW were quantified by conductometric titration using a conductometer (Metrohm 912, Switzerland) combined with pH monitoring using a pH meter (Orion Star A211, Thermo Fisher Scientific, USA). Dried nanomaterials were dispersed in double deionized water (~20 mL) in a 50-mL beaker followed by addition of HCl solution (1 M) dropwise until the pH of the suspensions reduced to <2. The resulting suspensions were stirred for 24 h to completely protonate surface groups. NaOH titrant solution (0.01 M) was added to the protonated suspensions using a syringe driver (Legato 200, KDSscientific, USA) at a rate of 0.05 mL min⁻¹. The conductivity and pH were continuously recorded at 30-s intervals and plotted against the volume of titrant added. Calculation of surface functional group contents is detailed in the Supporting Information.

2.4.4. Attenuated total reflectance Fourier-transform infrared spectroscopy

The infrared spectra of TCNF, ChNW, PP, and coated PP films were recorded using an FTIR spectrometer (Thermo Fisher Scientific Nicolet iS50, USA) with a spectral resolution of 0.09 cm⁻¹, equipped with a smart iTR diamond/ZnSe ATR accessory (face angle 45°). The spectra were obtained within 4000–700 cm⁻¹ range at a 4 cm⁻¹-scan step with 128 scans. The TCNF film sample (formed through water evaporation from the suspension) was immersed in HCl solution (0.01 M) to protonate the sodium salt (COONa) to the acid (COOH), then rinsed with deionized water, and dried prior to ATR-FTIR.

2.4.5. X-ray diffraction

The crystalline structures of TCNF and ChNW were studied using an

X-ray diffractometer (Rigaku RINT2000, Japan), equipped with a Ni-filtered Cu K α (λ of 1.542 Å) radiation, operating at 40 kV and 100 mA. The X-ray diffraction (XRD) patterns were obtained at 25 °C from 5° to 40° at a 1° min⁻¹-scan rate.

Peak fitting was performed using the Fit Peaks (Pro) function of OriginPro 8.5 program (OriginLab Co., USA) to deconvolute peaks and calculate peak intensity, from which the crystallinity indices (CI) of nanomaterials were determined. The CI of TCNF was calculated using the equation proposed by Segal et al. (1959), $CI (\%) = (I_{002} - I_{am})/I_{002} \times 100\%$, where I_{002} is the intensity (arbitrary unit) of the crystalline peak for the (002) plane at 2θ of 22.5°, and I_{am} is the peak intensity of the amorphous part at 2θ of ~18.0°. The CI of ChNW was calculated using the equation reported by Kumirska et al. (2010), $CI (\%) = (I_{110} - I_{am})/I_{110} \times 100\%$, where I_{110} is the intensity of the crystalline peak for the (110) plane at 2θ of 19.6°, and I_{am} is the peak intensity of the amorphous part at 2θ of ~12.6°.

2.4.6. Film thickness

The thickness of PP films was evaluated using an electronic digital micrometer (Mitutoyo, USA) with a sensitivity of 0.01 mm and reported as an average of at least three measurements.

2.4.7. UV-visible spectroscopy

The transmittance spectra within the UV-visible region (400–800 nm) of PP films (3 cm \times 5 cm) were obtained using a spectrometer (Shimadzu Corp. UV-2600, Japan), accessorized with a thin film holder compartment, at a resolution of 0.5 nm at 25 °C.

2.4.8. Static water contact angle

The hydrophilicity of PP films was evaluated through static water contact angles at 25 °C using a contact angle goniometer (Krüss GmbH DSA25, Germany). The drop volume used for the measurement was 5 μ L. The static contact angle was obtained after the water drop reached an equilibrium on the film surface by analyzing its macroscopic images using the built-in Advance program. The reported data were calculated from at least three measurements at different film locations.

2.4.9. Oxygen transmission rate

The OTR was measured at 23 °C and 50% relative humidity (RH) according to the ASTM D3985 standard using an automated oxygen permeability tester (Lyssy L100–5000, Systech Illinois Instruments Ltd., UK) (Nguyen et al., 2018). PP films were cut into circular shape of ~8 cm in diameter (test area of ~50 cm²) and firmly adhered to sample cards (Systech Illinois, UK). The cards were sealed between an upper chamber containing oxygen (99.999% purity) and a lower chamber void of oxygen. A coulometric sensor equipped in the lower chamber measures the oxygen volume permeated through unit area of PP films per unit time.

2.4.10. Water vapor transmission rate

The WVTR was measured following the ASTM E-96 standard (Nair et al., 2018). First, 100 g of deionized water was filled into a test permeability cup (Thwing-Albert EZ-Cup 68–3000, Germany). Subsequently, a circular PP film sample with a 6.4-cm diameter, sealed with a threaded ring flange between two gaskets, was attached to the cup. The test cup was placed in a temperature-humidity test chamber, preset at 30 °C and 50% RH using an equipped temperature and humidity controller (Temi1300, Samwon Tech, S. Korea). The weight of the cup was measured regularly (typically 8 days) until the slope of the weight loss curve became constant. WVTR was calculated from the water weight loss through the opening area of the cup over a specific time (Vahedikia et al., 2019; Jinwu Wang et al., 2018).

2.4.11. Tensile properties

The tensile test of PP samples was conducted using a universal testing machine (UTM, Instron 5943, Instron Corp., USA) equipped with a

1000-N load cell at a cross-head speed of 50 mm min⁻¹ (Parameswaranpillai et al., 2015). The films were cut into a dog-bone shape with following configurations—distance between grips, 26.5 mm; width of narrow section, 3.2 mm; and average thickness, 60 μ m. All samples were conditioned in a controlled-atmosphere chamber at 25 °C and 50% RH for 24 h before testing. Tensile data were reported as average values of five replicates.

2.4.12. Antibacterial activity

The antibacterial activities of pristine and (ChNW/TCNF)-coated PP films were evaluated using a previously reported method (Kim et al., 2019; Nguyen et al., 2016). The bacterial strains used in this experiment were Gram-negative *Escherichia coli* (DH5 α competent cells) and Gram-positive *Staphylococcus aureus* (Microbiologics CCARM 0078) obtained from Thermo Fisher Scientific (USA). Bacteria were first streaked on LB agar plates and allowed to grow at 37 °C. A single bacterial colony was then inoculated to LB broth, and the culture was grown in a shaking incubator (BioFree, S. Korea) at 37 °C, 180 rpm. The bacterial suspensions were harvested, diluted to an optical density at 600 nm (OD 600) of 0.6, and dropped (50 μ L) onto surfaces of circular film samples (7 mm in diameter). The films were incubated at 37 °C for 1 h, rinsed with deionized water, and immersed in fresh LB broth. The new cultures were incubated at 37 °C in a shaking incubator for 24 h, during which aliquots (~2 mL) were withdrawn every 2 h to measure the OD 600 and construct bacterial regrowth curves. Measurements for each film were done in triplicates using a spectrometer (Shimadzu Corp. UV-2600, Japan), accessorized with a cell (10-mm light path) compartment.

2.4.13. Thermal properties

The thermal degradation of PP films was characterized using a thermogravimetric analyzer (TGA, Pyris 1, PerkinElmer, USA). The films were preconditioned in a desiccator for 24 h for complete moisture removal. The dried films (~10 mg) were placed on a ceramic pan and heated from 25 °C to 800 °C at a rate of 10 °C min⁻¹ using a furnace under a dry N₂ purge flow of 50 mL min⁻¹.

Differential scanning calorimetry (DSC, TA Instrument Q2000, USA) was used to determine the glass-transition (T_g) and melting (T_m) temperatures of the films. Dried samples (~2 mg) were placed in the aluminum pan and subjected to three thermal scans—(1) heating from 25 to 200 °C, (2) cooling from 200 to -20 °C, and (3) heating back from -20 to 200 °C. All the thermal scans were performed at a rate of 20 °C min⁻¹ under a dry N₂ purge flow of 20 mL min⁻¹, and the samples were kept isothermal for 5 min at the beginning of each scan. The T_g and T_m values were determined from the second heating cycle (third thermal scan). In addition, the crystallinity (X) of the pristine PP film was calculated using the equation $X = 100 \times \Delta H_m / \Delta H_m^0$, where ΔH_m and ΔH_m^0 (171.1 J g⁻¹) are the melting enthalpies of pristine PP and theoretically 100% crystalline PP, respectively (Lanyi et al., 2020), and ΔH_m was obtained by integrating the melting peak area.

2.4.14. Melting behavior

Due to short-term nature of PP packaging products, thermal recycling of PP is a feasible solution to reduce its environmental pressure. Because the thermal recycling requires melting the polymer for further processing, we tested whether the coating layer affected the melting behavior and recyclability of PP films. Dried (ChNW/TCNF)-coated and aluminum-metalized PP films were heated on a hot plate at ~160 °C (T_m of PP determined from DCS), and the melting process of the films were observed.

3. Results and discussion

3.1. Morphology, surface feature, and colloidal stability of nanocellulose and nanochitin

TCNF has an average length of 544 nm and width of 14.1 nm with an

average aspect ratio of 38.5, whereas ChNW is 383 nm long and 33.0 nm wide on average, corresponding to an aspect ratio of 11.6 (Fig. 2a,b; Fig. S1, Supporting Information). These results agree with reported values for ChNW (Yongwang Liu et al., 2018) but vary for TCNF (Bakkari et al., 2019; Isogai et al., 2011; Kim et al., 2019) probably because of different cellulose sources used and procedures employed for TCNF production. Unfortunately, commercial TCNF used in our study is obtained using proprietary technology, and often the exact cellulose source, extraction and purification are not evident. The average COO⁻ content of TCNF is 1.40 mmol g⁻¹, which results from selective oxidation of primary hydroxyl groups (C6-OH) by TEMPO. ChNW has an NH₃⁺ content of 0.58 mmol g⁻¹ due to partial deacetylation by HCl at high temperature (Fig. S2 and Table S1, Supporting Information) (Bertuzzi et al., 2018; Revol & Marchessault, 1993). The pK_a of COOH is 3.6 (Fukuzumi et al., 2010); and NH₃⁺, 6.5 (H. Wang et al., 2011). Therefore, TCNF and ChW are well dispersed in water at pH 7 and 4, respectively, because their surface groups are ionized, which electrostatically stabilizes the suspension. This is indicated by a homogeneous transparency (TCNF) or translucency (ChNW) of the two suspensions without macroscopic aggregation and phase separation (Fig. 2c,d). It should be noted that the different appearance of the two suspensions may depend on factors including dimension (aspect ratio), surface charge density, and concentration of the dispersed materials (Reid et al., 2017). In addition, the ξ -potentials of TCNF (pH 7) and ChNW (pH 4) dispersions are -31.9 and +31.6 mV, respectively (Fig. 2e), comparable with literature data (Yongwang Liu et al., 2018; Qi et al., 2012). The absolute values are greater than 30 mV, typically considered the cutoff value required for colloidal stability (Kumar & Dixit, 2017).

3.2. Chemical and crystal structures of nanocellulose and nanochitin

Fig. 2f shows the ATR-FTIR spectra of TCNF and ChNW. The IR spectrum of TCNF exhibits typical bands (cm⁻¹) of cellulose, including 3305 (hydrogen-bonded O—H stretching), 2890 (C—H stretching), 1427

(CH₂ scissoring), 1372 (C—H bending), 1159 and 1054 (C—O stretching), and 898 (β -1,4-glycosidic linkage) (Yongliang Liu & Kim, 2015; Schramm, 2020). In addition, the 1717 cm⁻¹ band indicates the presence of —COOH groups successful converted from COONa groups by immersing the TCNF film into an acidic solution (Bakkari et al., 2019). The IR spectrum of ChNW shows signals (cm⁻¹) typical for α -chitin, comprising 3437 and 3259 (overlapped O—H and N—H stretching vibrations), 3104 (N—H stretching vibration), 2959–2875 (sp³-C—H stretching), 1653 (Amide I or C=O stretching in —CONH—), 1618 (stretching vibration of intermolecular hydrogen-bonded C=O), 1553 (Amide II including N—H bending and C—N stretching vibrations), and 1376–1203 (various types of C—H vibrations) (Ifuku et al., 2015; Ifuku et al., 2009; Yongwang Liu et al., 2018; Zając et al., 2015).

The X-ray diffraction patterns of the two nanomaterials are presented in Fig. 2g. The crystal structure of TCNF is characterized by 2 θ diffraction peaks at \sim 15, 17.5, and 22.5°, attributed to the (10), (110), and (002) crystallographic planes of cellulose I, respectively. The CI calculated for TCNF is \sim 63.01%, in reasonable agreement with literatures (Bakkari et al., 2019; Tang et al., 2017). The result suggests that TEMPO treatment negligibly affects the original crystal structure of cellulose, probably due to the insolubility and low accessibility of cellulose to reagents in aqueous media (Isogai et al., 2011). ChNW exhibits diffraction peaks at 2 θ of 9.5, 19.4, 21.4, 23.7, and 26.7°, indexed as (020), (110), (101), (130), and (013) crystallographic planes of α -chitin, respectively (Y. Lu et al., 2013). The CI of ChNW was determined to be \sim 95.48% due to depolymerization and removal of α -chitin amorphous region by HCl. The value is well matched with previous reported data by T. H. Tran et al. (2019).

3.3. Layer-by-layer assembly of nanocellulose and nanochitin on polypropylene films

The coating method used in this study was LbL assembly, which has been widely employed to fabricate thin coating layers with controlled

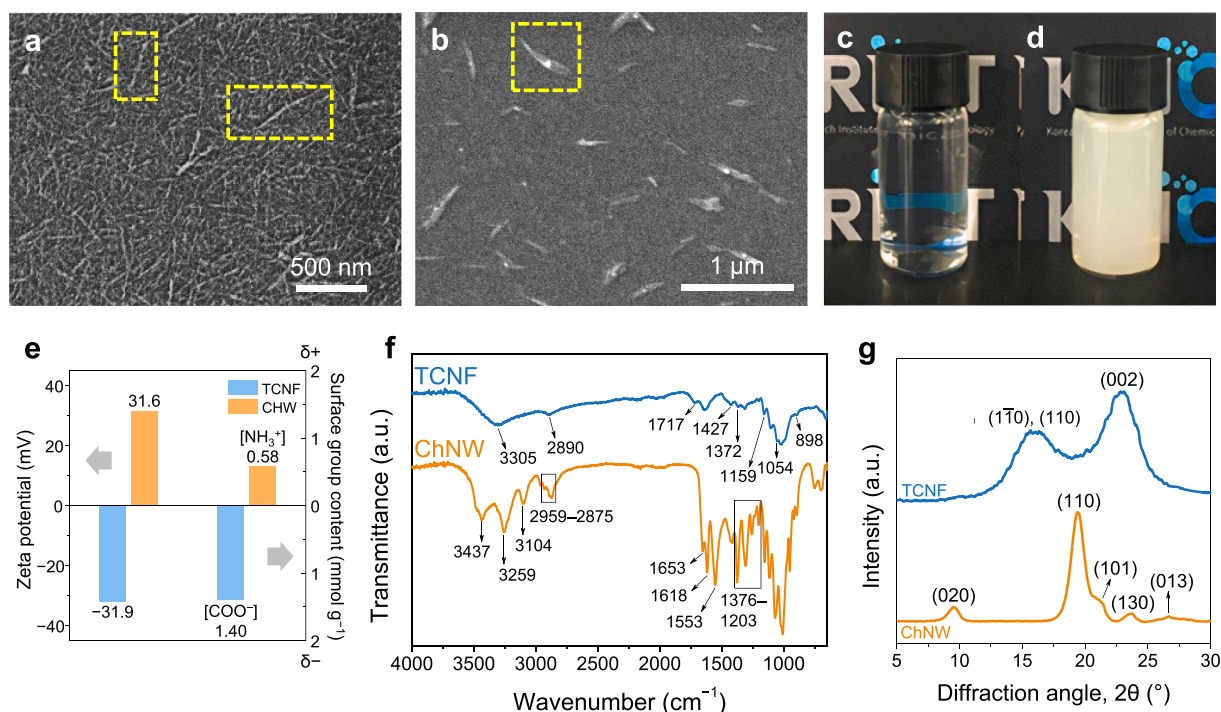


Fig. 2. Characterization of nanomaterials. FE-SEM images of (a) TCNF and (b) ChNW showing individualized nanofibers/nanowhiskers in dash yellow boxes. Optical photographs of (c) TCNF (0.4 wt%, pH 7) and (d) ChNW (1.6 wt%, pH 4) aqueous suspensions showing their colloidal stability. (e) Zeta potentials of TCNF and ChNW aqueous suspensions at pH 7 and 4, respectively, and surface functional group contents of TCNF and ChNW, (f) ATR-FTIR spectra and (g) XRD patterns of TCNF and ChNW verifying their chemical and crystal structures.

structure and composition on a substrate surface (Ferrer et al., 2017). LbL assembly is achieved through an alternate deposition of different functional materials to construct the coating layer, which is usually based on strong electrostatic interactions of oppositely charged coating components (Cazón et al., 2017; de Mesquita et al., 2010; Marais et al., 2014; Qi et al., 2012; Wågberg et al., 2008; Yagoub et al., 2014). TCNF and ChNW were LbL-assembled onto the PP film surface through dip coating. This coating technique is simple, inexpensive and can form LbL assemblies on both sides of PP films simultaneously. It also performs well with lowly viscous aqueous nanomaterial suspensions and yields excellent reproducibility (Richardson et al., 2016).

The colloidal stability of TCNF and ChNW (Fig. 2c–e) enables a uniform formation of the barrier layer on PP films by dip coating. Moreover, their opposite surface charges and different aspect ratios leads to formation of consecutive tightly bonded layers (Kim et al., 2019). Indeed, the SEM images (Fig. 3b) shows 20 stable bilayers of (ChNW/TCNF) tightly adhering to the PP surface with no significant defect. The thickness of 20 bilayers is $\sim 7 \mu\text{m}$; therefore, one (ChNW/TCNF) bilayer is $\sim 350 \text{ nm}$ thick on average.

The strong adhesion of coating layers to PP films is a result of treating the pristine PP surface with UVO. The irradiation cleaved C–C and C–H bond and produced free radicals and hydrophilic groups. As evidence, the ATR-FTIR spectrum of UVO-treated PP films show a reduction in the

intensity of signals at 2990–2820, 1452–1376, 1167, and 997–809 cm^{-1} (various C–C and C–H vibrations) and the presence of a C=O stretching vibration band at 1713 cm^{-1} (Fig. S3, Supporting Information) (d'Eon et al., 2017; Hedrick & Chuang, 1998; C. T. H. Tran et al., 2016). Increased hydrophilicity of UVO-treated PP films was also verified with a decrease in the water contact angle from 103 to 62.4° (Fig. 3c). The generated species on the PP surface bear (partially) negative charges, which facilitate the strong adhesion of the first coating layer (positively charged ChNW) through electrostatic attraction.

Upon coating, the water contact angle drops to $< 30^\circ$ owing to the hydrophilicity of nanomaterials (Fig. 3c). Furthermore, the IR spectrum of PP film coated with 20 ChNW/TCNF bilayers shows additional bands at 3430–3102, 1656, 1621, and 1558 cm^{-1} of cellulose I and α -chitin (Ifuku et al., 2015; Yongliang Liu & Kim, 2015; Yongwang Liu et al., 2018; Schramm, 2020; Zajac et al., 2015), suggesting that both nanomaterials were successfully deposited onto the PP surface (Fig. 3d). In order word, a following dip coating cycle did not remarkably abrade previously adhered nanomaterials, showcasing the efficiency of immersion coating, up to 20 cycles.

The coated PP film exhibited high transparency, similar to the pristine PP film (Fig. 3e). The transmittance of both pristine and 20 BL-coated PP films within the UV–visible region (400–800 nm) were 87–100% (Fig. 3f). These results suggest that the stacked-up coating

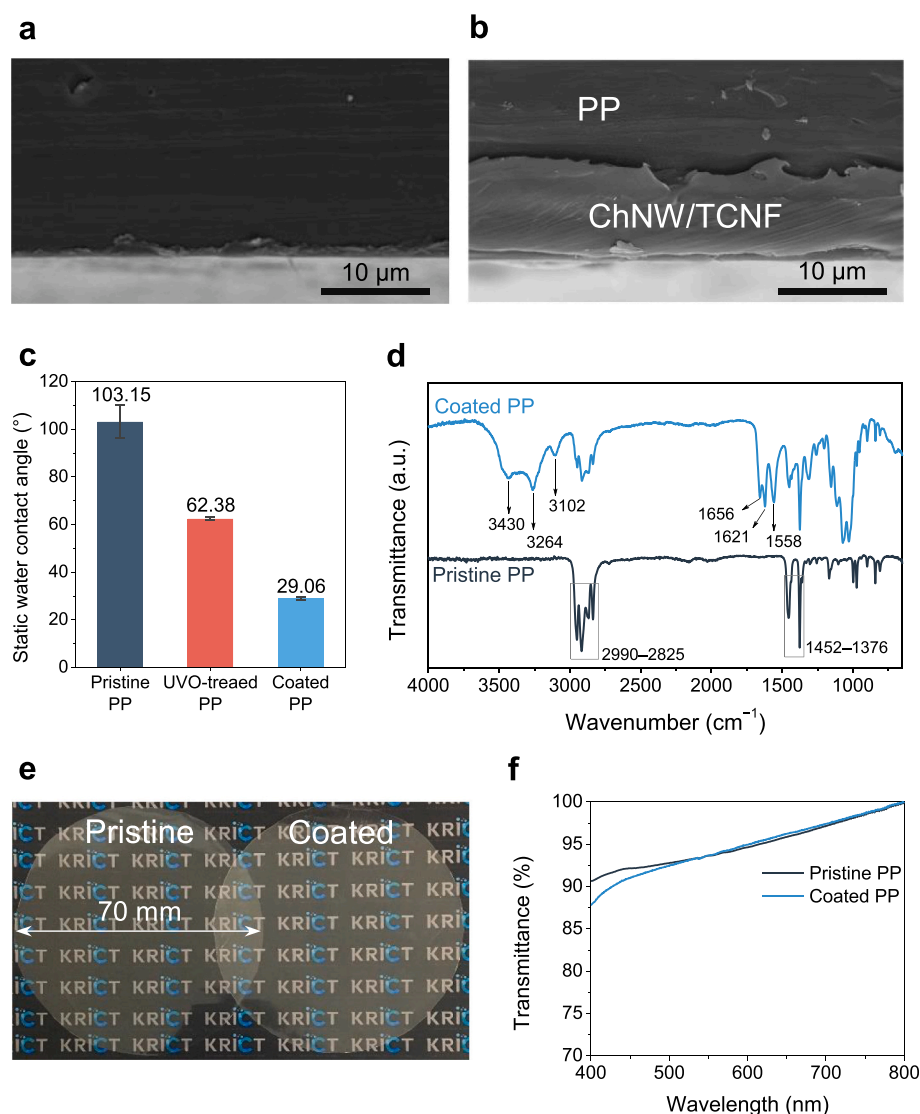


Fig. 3. Characterization of the pristine PP film and PP film coated with 20 bilayers of nanomaterials through dip coating in suspensions of ChNW (1.6 wt %, pH 4) and TCNF (0.4 wt%, pH 7). FE-SEM images showing the cross section of (a) pristine and (b) coated PP films. (c) Static water contact angles of PP, UVO-treated PP (20 min), and coated PP films. Data are expressed as means and standard deviations of triplicates ($n = 3$). (d) ATR-FTIR spectra of pristine and coated PP films. (e) Optical photographs showing the high transparency of both films, allowing a clear view of the content behind, and (f) their transmittance spectra in the UV–visible region.

layers are highly transparent owing to the conversion of bulk cellulose and chitin into nano-scaled materials without aggregation (Isogai et al., 2011; T. H. Tran et al., 2019). Transparency is one of the most important properties of food packaging materials because it allows the consumers to view and evaluate the content inside (Cazón et al., 2018; Sun et al., 2019; Vasile, 2018). In addition, transparent materials can easily be integrated with other optical sensing systems, such as radio frequency sensors, for the development of intelligent food packaging materials that can monitor food freshness (Kiriyukhin et al., 2018).

3.4. Layer-by-layer nanocellulose/nanochitin-coated polypropylene films as a high-performance food packaging material

High-performance packaging materials need to show excellent barrier properties to atmospheric penetrants (oxygen gas and water vapor), good mechanical performance, and other high-order properties such as antibacterial and favorable thermal properties. To this end, the pristine and LbL-(ChNW/TCNF)-coated PP films were compared for their food packaging application potentials.

We first optimized the concentrations of the two nanomaterial suspensions and the number of bilayers (number of dip coating cycles) to obtain the highest gas barrier performance. We found that the OTR of LbL-coated PP films (60 μm thick) reached a minimum of 13.10 $\text{cc m}^{-2} \text{day}^{-1}$ at 20 bilayers using 0.4 wt% TCNF and 1.6 wt% ChNW suspensions (Fig. 4a; Fig. S4, Supporting Information). This value represents nearly a hundredfold reduction compared with the pristine PP film with

the same thickness (1117.51 $\text{cc m}^{-2} \text{day}^{-1}$).

Generally, a good alignment of crystalline, high-aspect-ratio materials like TCNF and ChNW is necessary to improve the gas barrier performance of coated PP films. This creates a “tortuous pathway” that directs the gas molecules around impermeable crystalline parts, increasing their diffusion time (Cacciotti et al., 2018; Cacciotti & Nanni, 2016; Kim et al., 2019; Priolo et al., 2011). To attain a desired alignment of TCNF and ChNW in the coating layer, we propose that the charge density of the two nanomaterials needs to be balanced. Assuming a cylinder shape for both nanomaterials, the surface area of TCNF is ~ 1.7 times smaller than that of ChNW. However, as TCNF has 2.4 times higher surface functional group concentration than ChNW, the charge density (per surface area) of TCNF is ~ 4.1 times larger than that of ChNW. Therefore, to achieve the charge balance, the concentration of ChNW suspension should be roughly four times higher than that of TCNF, theoretically. It should also be emphasized that the concentration of TCNF suspension needs to be sufficiently high to achieve an essential coverage on PP film surface for a high barrier performance (Fig. S4a, Supporting Information).

When the concentration of TCNF suspension was fixed at 0.4 wt%, increasing the concentration of ChNW suspension from 0.8 to 1.6 wt% brought the charge density of the two materials closer to balance, leading to a better alignment and deposition of ChNW with respect to TCNF. A greater amount of uniformly distributed, shorter ChNW can fill local voids created by longer TCNF (Kim et al., 2019). This produces a thicker and more tightly packed coating layer, hence an improved

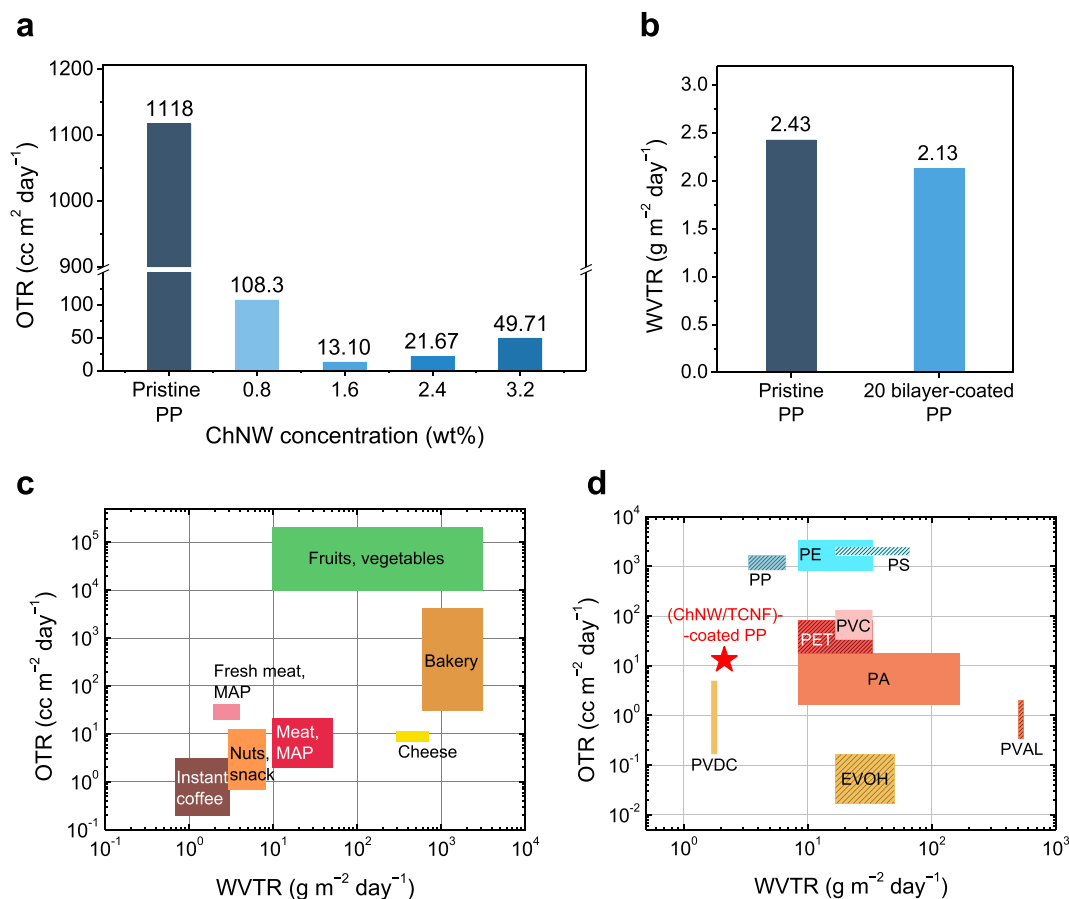


Fig. 4. Barrier performance of the pristine PP film and PP film coated with 20 (ChW/TCNF) bilayers. (a) OTR of the pristine PP film and coated films through dip coating in the TCNF suspension (0.4 wt%, pH 7), and ChNW suspensions (pH 4) at various concentrations. (b) WVTR of the pristine film and 20 bilayer-coated film using TCNF 0.4 wt% and ChNW 1.6 wt% suspensions. (c) OTR and WVTR requirements for various types of food products (Stocchetti, 2012); MAP, modified atmosphere packaging. (d) Comparing the barrier performance of the (ChNW/TCNF)-coated PP film in this study with those of some common polymers used in food packaging including PET: poly(ethylene terephthalate); PP, polypropylene; PE, polyethylene; PS, polystyrene; PVC, poly(vinyl chloride); PA, polyamide; PVAL, poly(vinyl alcohol); EVOH, ethylene vinyl alcohol; and PVDC, poly(vinylidene chloride) (Lange & Wyser, 2003). Data are normalized for 60 μm -thick film.

oxygen barrier performance in the coated PP films (Priolo et al., 2010; Yu et al., 2019). Higher ChNW concentrations (2.4 and 3.2 wt%) are more viscous and result in an exceed positive charge density. Therefore, ChNW experiences more repulsion force at the coating layer–liquid interface and is unable to bind and align well to TCNF. The resulting coating layers are more prone to oxygen permeability and show an increase in OTR (Fig. 4a). Owing to its best barrier performance, 20 bilayer-coated PP films using TCNF (0.4 wt%) and ChNW (1.6 wt%) suspensions were used for subsequent tests, unless noticed.

In addition, to showcase the robust reproducibility of the dip coating technique, we assembled 20 (ChNW/TCNF) bilayers on a PP film with a greater thickness of 180 μm . The resulting composite film showed a reduction of two orders of magnitude in OTR from 308.2 to 3.5 $\text{cc m}^{-2} \text{day}^{-1}$ (Fig. S5, Supporting Information).

The WVTR of the film is one of the key parameters for evaluating the performance of a material as a barrier packaging (P. Lu et al., 2018; Jinwu Wang et al., 2018). Without packaging, foods gain or lose moisture until they reach equilibrium with the RH of the environment. The WVTR of the pristine and 20 bilayer-coated PP films are similar (2.43, and 2.13 $\text{g m}^{-2} \text{day}^{-1}$, respectively (Fig. 4b). The inherent water sensitivity of hydrophilic materials like cellulose and chitin can be compensated by the great moisture barrier of PP. As a result, our composite of bio-based coating and petroleum-based substrate exhibits dual barrier properties that meet the OTR and WVTR requirements for most groups of food products and are competitive with conventional polymeric packaging (Fig. 4c,d).

Food packages should be mechanically robust to effectively protect the food inside. Tensile testing results (Fig. 5) show that coating slightly

reduced mechanical properties of composite films. The 20 bilayer-coated PP film exhibited a $\sim 6\%$ increase in Young's modulus (from 1.29 to 1.37 GPa) but a noticeably lower tensile strength (29 MPa) and elongation at break (367%) compared with the pristine PP films (46 MPa and 636%, respectively). The mechanical properties of (ChNW/TCNF)-coated PP films can be understood by considering that adhering two mechanically different materials may result in stress concentration that initiates cracking at the interface (Dagleish et al., 1989). The stiffness of highly crystalline cellulose I and α -chitin is 130 GPa and 40–60 GPa, respectively (Araki et al., 2012; Guan et al., 2020; Ogawa et al., 2011), much higher than PP (~ 1.3 GPa). By contrast, the elongation at break of both nanomaterials is $<10\%$, 60 times smaller than that of PP (636%), indicating that TCNF and ChNW are brittle, whereas PP is ductile. Upon coating, TCNF and ChNW exhibits volume and thermal contraction during drying at 80 $^{\circ}\text{C}$ (Section 2.3). This introduces a large residual stress at the PP–ChNW interface, which can adversely affect the mechanical properties of the substrate. The failure of the brittle ChNW/TCNF coating layer can pinpoint a stress in the adjacent PP layer, causing an early failure of the composite (Abadias et al., 2018). We note that UVO irradiation is unlikely to reduce the mechanical properties of the coated PP films because it only penetrates few nanometers deep without changing bulk properties of the film (as evident by the ATR-FTIR spectra in Fig. S3, Supporting Information). Despite the trade-off for gaining the barrier function, all the coated films show mechanical properties comparable with commercial polymers used in the packaging industry (Sangroniz et al., 2019).

Antibacterial properties are another attractive function of food packaging materials. Therefore, we investigated the antibacterial

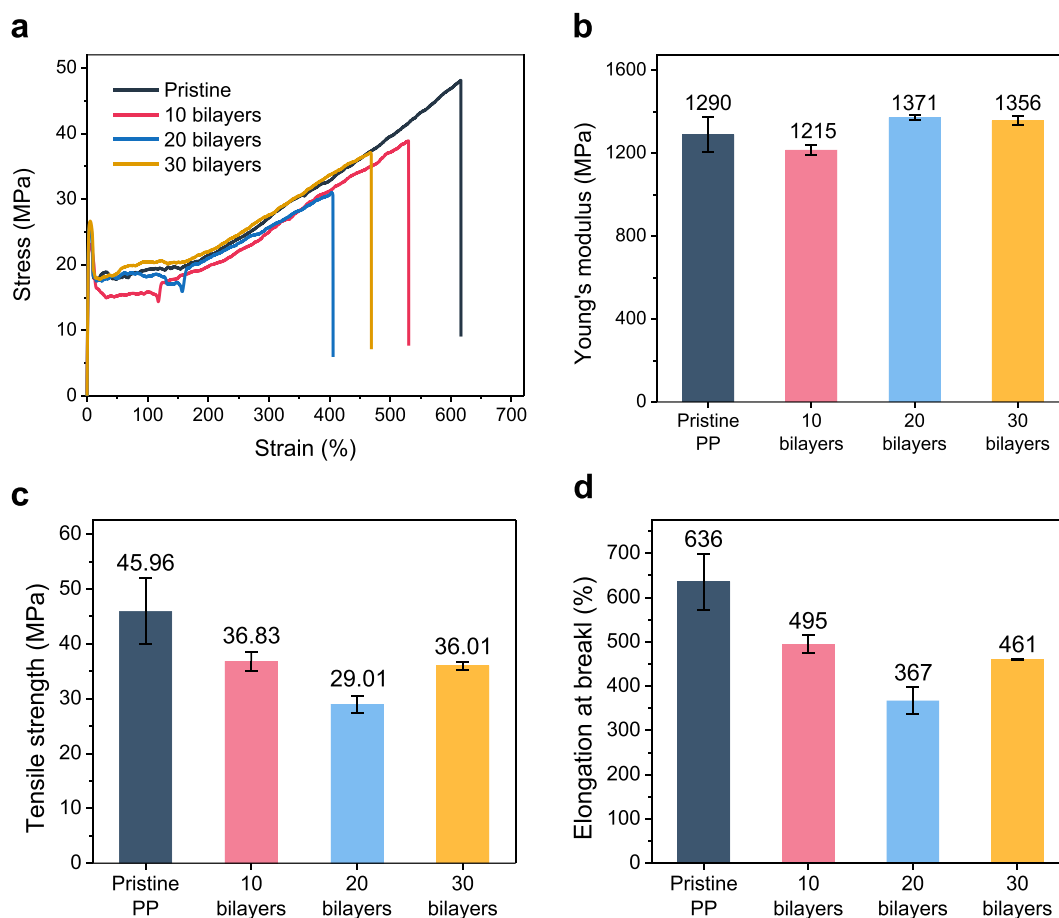


Fig. 5. Mechanical properties including (a) representative tensile stress–strain curves, (b) Young's modulus, (c) tensile strength, and (d) elongation at break of the pristine PP film and (ChNW/TCNF)-coated PP films with different numbers of coating bilayers. Coating suspensions are 1.6 wt% ChNW at pH 4 and 0.4 wt% TCNF at pH 7. Data are expressed as means \pm standard deviations of five replicates.

properties of pristine and coated PP films against Gram-negative *Escherichia coli* and Gram-positive *Staphylococcus aureus*. The bacteria upon contacting the films were incubated in culture media, and their regrowth curves were monitored through OD 600 readings. The growth kinetics of both bacteria exposed to the coated PP films was slower than that of bacteria exposed to the pristine PP film at virtually all investigating time points, suggesting that the coated film initially has fewer attached bacterial cells than the pristine film (Fig. 6). Hence, the ChNW/TCNF coating layer can reduce the bacterial adhesion and biofilm formation on the composite film surface.

It has been established that the antibacterial effects of chitin/chitosan-based materials are attributed to the protonated amino (NH_3^+) group. The group strongly binds to negatively charged sites on the cytoplasmic membrane or cell wall of bacteria and disrupts their organization and permeability, inducing leakage of intracellular content and cell death (Arkoun et al., 2017; Kim et al., 2019; T. H. Tran et al., 2019). We observed that *S. aureus* was more sensitive to ChNW activity than *E. coli* possibly because the outer membrane of Gram-negative bacteria provides an additional protection against ChNW (Coma et al., 2003). However, the antibacterial effectiveness and mechanism of chitin/

chitosan-based materials are host-dependent and widely debated topics (Sahariah & Måsson, 2017) that are beyond the scope of this study. Negatively charged COO^- groups of TCNF can screen the positively charged NH_3^+ groups and reduce the antibacterial effect of ChNW, which explains the moderate but incomplete elimination of bacterial on coated PP films (Kim et al., 2019; T. H. Tran et al., 2019). Nevertheless, a low cell adhesion can extend the growth phase of microorganisms and prolong the shelf life of food products (Biji et al., 2015).

The thermal properties of pristine and LbL ChNW/TCNF-coated PP films are summarized in Fig. 7. TGA results reveal that 20 bilayers of nanocellulose and nanochitin deposited onto PP can retard the thermal degradation of the substrate owing to their high crystallinity. The decomposition temperature at 5% weight loss (T_{45}) of the coated PP film increased by $\sim 60^\circ\text{C}$ compared with the pristine film (Fig. 7a). First-order derivatives of the TGA curves show that the pristine film decomposes more abruptly at the maximum decomposition temperature (T_{max}) of 422°C , whereas the coated film decomposed more slowly at a higher T_{max} of 466°C (Fig. S6, Supporting Information).

DSC thermograms show that both films have similar glass transition temperatures (T_g of about -17 to -16°C) and melting temperatures (T_m of $\sim 160^\circ\text{C}$) (Fig. 7b). The melting enthalpy (ΔH_m) of the neat PP was determined to be 94.43 J g^{-1} , corresponding to a crystallinity X of 55.19% (Section 2.4.13), in good agreement with a previous study (Díez et al., 2005). We emphasize that this approach cannot be applied for the coated PP film although it is expected that the crystallinity of PP is not affected by either UVO treatment or dip coating. The coated sample comprises thermally different adhered materials, and the poor heat conductivity of cellulose and chitin (Sato et al., 2020; Jiahao Wang et al., 2021) isolates the inner PP film from absorbing heat. As a result, the composite film requires more thermal energy to melt the PP crystal, resulting in a larger apparent melting enthalpy.

There has been increasing concern over the sustainability and recyclability of next-generation plastics (Park et al., 2019; Schneiderman & Hillmyer, 2017). Particularly, the demand for single-use plastics has been dramatically increased recently in the COVID-19 pandemic (Prata et al., 2020). To reduce the environmental burdens introduced by short-term plastics like PP, it is important to recycle PP. After properly sorting and cleaning, the recycling of PP involves melting, extrusion, and pelletizing to manufacture other products. PP can also be recovered via pyrolysis to become liquid fuels (Butler et al., 2011). Therefore, it is ideal that the coating layer does not significantly affect the melting behavior of the PP substrate. We show that PP coated using nanocellulose and nanochitin can meet the current sustainability trend because it is meltable, hence recyclable, as opposed to aluminum-metalized PP (Fig. 7c,d).

4. Conclusion

We developed an LbL assembly of negatively charged TCNF and positively charged ChNW on polypropylene films using dip coating. Concentrations of the two coating nanomaterial suspensions are optimized to obtain a high gas-barrier performance. The $60\text{ }\mu\text{m}$ -thick PP film coated with 20 alternating bilayers of TCNF (0.4 wt%) and ChNW (1.6 wt%) exhibits an OTR of $13.1\text{ cc m}^{-2}\text{ day}^{-1}$, representing a two orders of magnitude reduction compared with the pristine PP film. Its WVTR maintains at $2.13\text{ g m}^{-2}\text{ day}^{-1}$, which is not affected by the coating layers. The barrier performance can meet packing requirements for most food products and is comparable with many commercially benchmarked petroleum-based polymer packaging. Furthermore, the ChNW/TCNF-coated PP film is highly transparent ($>87\%$) and can prevent bacterial adhesion to a moderate extent. The composite film also exhibits required mechanical robustness, and high thermal recyclability over aluminum-metalized packaging. Given the natural abundance and bio-renewability of the coating materials combining with the versatility of dip coating-mediated LbL assembly, we are aware that this approach can advance the food packaging industry towards high-performance,

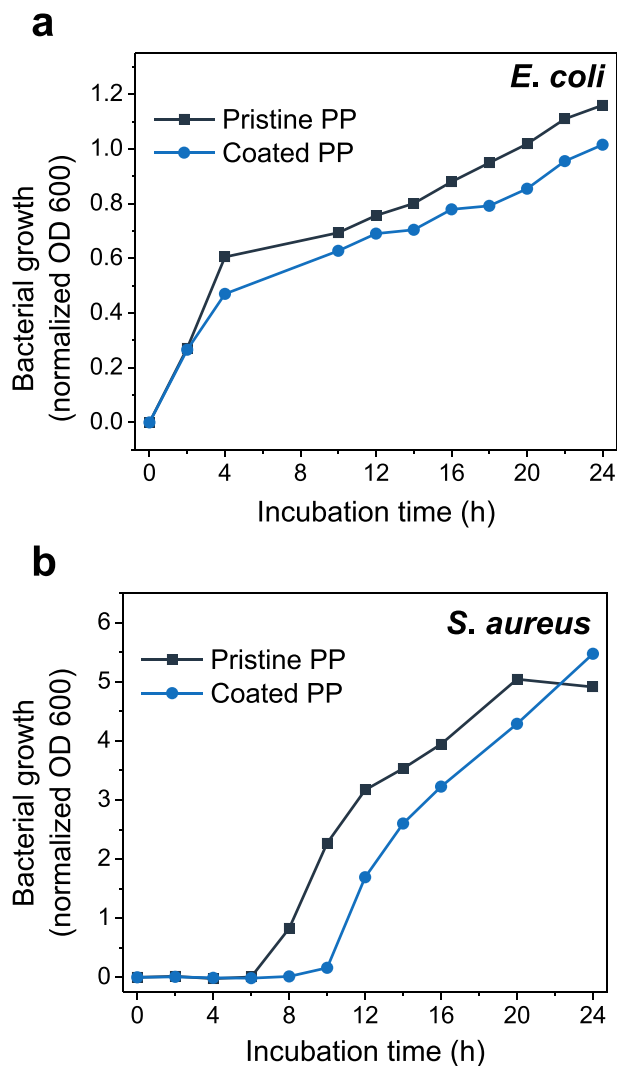


Fig. 6. Antibacterial adhesion of the pristine PP film and PP film coated with 20 bilayers of ChNW (1.6 wt%, pH 4) and TCNF (0.4 wt%, pH 7). Bacteria including (a) Gram-negative *Escherichia coli* DH5 α and (b) Gram-positive *Staphylococcus aureus* exposed to the films were regrown in lysogeny broth, pH 7.0 at 37°C , and their growth curves were monitored over time through optical density at 600 nm.

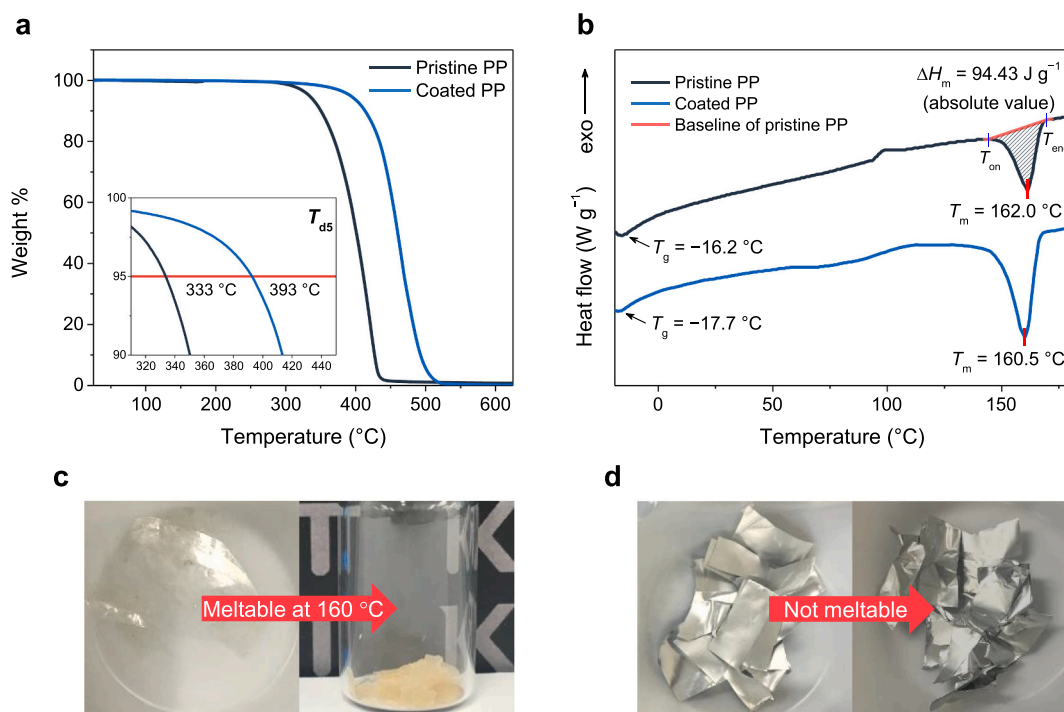


Fig. 7. Thermal properties of the pristine PP film and PP film coated with 20 (ChW/TCNF) bilayers. Coating suspensions are 1.6 wt% ChNW at pH 4 and 0.4 wt% TCNF at pH 7. (a) TGA curves showing their degradation behaviors in N₂ gas. (b) DSC thermograms of the 3rd thermal scan (2nd heating) of the films in N₂ gas; T_g , glass-transition temperature; T_m , melting temperature; T_{on} and T_{end} , onset and ending temperatures of the melting, respectively. Integration of the melting peak yields melting enthalpy (ΔH_m , shaded area) of the pristine PP films. (c) The (ChNW/TCNF)-coated PP films can be melted at ~ 160 °C, but (d) aluminum-metalized PP films cannot be melted under the same condition.

multifunctional, and sustainable materials that can meet the globally increasing demand for green products.

CRediT authorship contribution statement

Hoang-Linh Nguyen: Methodology, Validation, Formal analysis, Data curation, Writing – original draft, Visualization. **Thang Hong Tran:** Methodology, Validation, Formal analysis. **Lam Tan Hao:** Formal analysis, Writing – review & editing, Visualization. **Hyeonyeol Jeon:** Validation, Investigation. **Jun Mo Koo:** Resources, Validation. **Giyoung Shin:** Methodology, Visualization. **Dong Soo Hwang:** Conceptualization, Supervision, Project administration. **Sung Yeon Hwang:** Conceptualization, Supervision, Project administration, Funding acquisition. **Jeyoung Park:** Conceptualization, Supervision, Project administration, Funding acquisition. **Dongyeop X. Oh:** Conceptualization, Writing – review & editing, Supervision, Project administration, Funding acquisition.

Declaration of competing interest

The authors declare no conflict of interest.

Acknowledgments

This article is dedicated to the memory of Dr. Hoang-Linh Nguyen, who left us recently. All KRICT and POSTECH members will remember him forever. We are also grateful to the Korea Research Institute of Chemical Technology (KRICT) Core Projects for its support.

Appendix A. Supplementary data

Supplementary data to this article can be found online at <https://doi.org/10.1016/j.carbpol.2021.118421>.

References

- Abadias, G., Chason, E., Keckes, J., Sebastiani, M., Thompson, G. B., Barthel, E., et al. (2018). Review article: Stress in thin films and coatings: Current status, challenges, and prospects. *Journal of Vacuum Science & Technology A: Vacuum, Surfaces, and Films*, 36(2), Article 020801. <https://doi.org/10.1116/1.5011790>
- Abbaszadeh, M., Krizak, D., & Kundu, S. (2019). Layer-by-layer assembly of graphene oxide nanoplatelets embedded desalination membranes with improved chlorine resistance. *Desalination*, 470, Article 114116. <https://doi.org/10.1016/j.desal.2019.114116>
- Allahvaysi, S. (2012). Polypropylene in the industry of food packaging. In F. Dogan (Ed.), *Polypropylene* (pp. 3–22).
- Araki, J., Yamanaka, Y., & Ohkawa, K. (2012). Chitin-chitosan nanocomposite gels: Reinforcement of chitosan hydrogels with rod-like chitin nanowhiskers. *Polymer Journal*, 44(7), 713–717. <https://doi.org/10.1038/pj.2012.11>
- Arkoun, M., Daigle, F., Heuzey, M. C., & Aiji, A. (2017). Antibacterial electrospun chitosan-based nanofibers: A bacterial membrane perforator. *Food Science and Nutrition*, 5(4), 865–874. <https://doi.org/10.1002/fsn3.468>
- Bakkari, M. E., Bindiganavile, V., Goncalves, J., & Boluk, Y. (2019). Preparation of cellulose nanofibers by TEMPO-oxidation of bleached chemi-thermomechanical pulp for cement applications. *Carbohydrate Polymers*, 203, 238–245. <https://doi.org/10.1016/j.carbpol.2018.09.036>
- Bertuzzi, D. L., Becher, T. B., Capreti, N. M. R., Amorim, J., Jurberg, I. D., Megiatto, J. D., & Ornelas, C. (2018). General protocol to obtain D-glucosamine from biomass residues: Shrimp shells, cicada sloughs and cockroaches. *Global Challenges*, 2(11), Article 1800046. <https://doi.org/10.1002/gch2.201800046>
- Biji, K. B., Ravishankar, C. N., Mohan, C. O., & Srinivasa Gopal, T. K. (2015). Smart packaging systems for food applications: A review. *Journal of Food Science and Technology*, 52(10), 6125–6135. <https://doi.org/10.1007/s13197-015-1766-7>
- Boyes, W. K., & Van Thriel, C. (2020). Neurotoxicology of nanomaterials. *Chemical Research in Toxicology*, 33(5), 1121–1144. <https://doi.org/10.1021/acs.chemrestox.0c00050>
- Butler, E., Devlin, G., & McDonnell, K. (2011). Waste polyolefins to liquid fuels via pyrolysis: Review of commercial state-of-the-art and recent laboratory research. *Waste and Biomass Valorization*, 2(3), 227–255. <https://doi.org/10.1007/s12649-011-9067-5>
- Cacciotti, I., Fortunati, E., Puglia, D., Kenny, J. M., & Nanni, F. (2014). Effect of silver nanoparticles and cellulose nanocrystals on electrospun poly(lactic acid) mats: Morphology, thermal properties and mechanical behavior. *Carbohydrate Polymers*, 103(1), 22–31. <https://doi.org/10.1016/j.carbpol.2013.11.052>
- Cacciotti, I., Mori, S., Cherubini, V., & Nanni, F. (2018). Eco-sustainable systems based on poly(lactic acid), diatomite and coffee grounds extract for food packaging.

- International Journal of Biological Macromolecules*, 112, 567–575. <https://doi.org/10.1016/j.ijbiomac.2018.02.018>
- Cacciotti, I., & Nanni, F. (2016). Poly(lactic) acid fibers loaded with mesoporous silica for potential applications in the active food packaging. *AIP Conference Proceedings*, 1738, Article 270018. <https://doi.org/10.1063/1.4952057>
- Cai, H., Wang, P., & Zhang, D. (2019). pH-responsive linkages-enabled layer-by-layer assembled antibacterial and antiadhesive multilayer films with polyelectrolyte nanocapsules as biocide delivery vehicles. *Journal of Drug Delivery Science and Technology*, 54, Article 101251. <https://doi.org/10.1016/j.jddst.2019.101251>
- Cazón, P., Vázquez, M., & Velázquez, G. (2018). Cellulose-glycerol-polyvinyl alcohol composite films for food packaging: Evaluation of water adsorption, mechanical properties, light-barrier properties and transparency. *Carbohydrate Polymers*, 195, 432–443. <https://doi.org/10.1016/j.carbpol.2018.04.120>
- Cazón, P., Velázquez, G., Ramírez, J. A., & Vázquez, M. (2017). Polysaccharide-based films and coatings for food packaging: A review. *Food Hydrocolloids*, 68, 136–148. <https://doi.org/10.1016/j.foodhyd.2016.09.009>
- Coma, V., Deschamps, A., & Martial-Gros, A. (2003). Bioactive packaging materials from edible chitosan polymer—Antimicrobial activity assessment on dairy-related contaminants. *Journal of Food Science*, 68(9), 2788–2792. <https://doi.org/10.1111/j.1365-2621.2003.tb05806.x>
- d'Eon, J., Zhang, W., Chen, L., Berry, R. M., & Zhao, B. (2017). Coating cellulose nanocrystals on polypropylene and its film adhesion and mechanical properties. *Cellulose*, 24(4), 1877–1888. <https://doi.org/10.1007/s10570-017-1222-0>
- Dalgleish, B. J., Trumble, K. P., & Evans, A. G. (1989). The strength and fracture of alumina bonded with aluminum alloys. *Acta Metallurgica*, 37(7), 1923–1931. [https://doi.org/10.1016/0001-6160\(89\)90077-1](https://doi.org/10.1016/0001-6160(89)90077-1)
- de Mesquita, J. P., Donnici, C. L., & Pereira, F. V. (2010). Biobased nanocomposites from layer-by-layer assembly of cellulose nanofibers with chitosan. *Biomacromolecules*, 11(2), 473–480. <https://doi.org/10.1021/bm9011985>
- Decher, G., & Hong, J. D. (1991). Buildup of ultrathin multilayer films by a self-assembly process: II. Consecutive adsorption of anionic and cationic bipolar amphiphiles and polyelectrolytes on charged surfaces. *Berichte der Bunsengesellschaft für Physikalische Chemie*, 95(11), 1430–1434. <https://doi.org/10.1002/bbpc.19910951122>
- Díez, F. J., Alvarino, C., López, J., Ramírez, C., Abad, M. J., Cano, J., et al. (2005). Influence of the stretching in the crystallinity of biaxially oriented polypropylene (BOPP) films. *Journal of Thermal Analysis and Calorimetry*, 81(1), 21–25. <https://doi.org/10.1007/s10973-005-0739-x>
- Ferrer, A., Pal, L., & Hubbe, M. (2017). Nanocellulose in packaging: Advances in barrier layer technologies. *Industrial Crops and Products*, 95, 574–582. <https://doi.org/10.1016/j.indcrop.2016.11.012>
- Fukuzumi, H., Saito, T., Okita, Y., & Isogai, A. (2010). Thermal stabilization of TEMPO-oxidized cellulose. *Polymer Degradation and Stability*, 95(9), 1502–1508. <https://doi.org/10.1016/j.polymdegradstab.2010.06.015>
- Garavand, F., Cacciotti, I., Vahedikia, N., Salara, A. R., Tarhan, Ö., Akbari-Alavijeh, S., et al. (2020). A comprehensive review on the nanocomposites loaded with chitosan nanoparticles for food packaging. *Critical Reviews in Food Science and Nutrition*, 1–34. <https://doi.org/10.1080/10408398.2020.1843133>
- Garavand, F., Rouhi, M., Razavi, S. H., Cacciotti, I., & Mohammadi, R. (2017). Improving the integrity of natural biopolymer films used in food packaging by crosslinking approach: A review. *International Journal of Biological Macromolecules*, 104, 687–707. <https://doi.org/10.1016/j.ijbiomac.2017.06.093>
- Grand View Research. (2020). Plastic packaging market size, share & trends analysis report by product (bottles, bags, wraps & films), by type (rigid, flexible), by application (food & beverages, industrial), and segment forecasts, 2020–2027. Retrieved from <https://www.grandviewresearch.com/industry-analysis/plastic-packaging-market> (Accessed 28 Apr, 2021).
- Guan, Q.-F., Yang, H.-B., Han, Z.-M., Zhou, L.-C., Zhu, Y.-B., Ling, Z.-C., ... Yu, S.-H. (2020). Lightweight, tough, and sustainable cellulose nanofiber-derived bulk structural materials with low thermal expansion coefficient. *Science Advances*, 6(18), eaaz1114. doi:<https://doi.org/10.1126/sciadv.aaz1114>
- Halakoo, E., & Feng, X. (2020). Layer-by-layer assembly of polyethyleneimine/graphene oxide membranes for desalination of high-salinity water via pervaporation. *Separation and Purification Technology*, 234, Article 116077. <https://doi.org/10.1016/j.seppur.2019.116077>
- Hedrick, S. A., & Chuang, S. S. C. (1998). Temperature programmed decomposition of polypropylene: In situ FTIR coupled with mass spectroscopy study. *Thermochimica Acta*, 315(2), 159–168. [https://doi.org/10.1016/S0040-6031\(98\)00283-4](https://doi.org/10.1016/S0040-6031(98)00283-4)
- Heo, J., Choi, M., & Hong, J. (2019). Facile surface modification of polyethylene film via spray-assisted layer-by-layer self-assembly of graphene oxide for oxygen barrier properties. *Scientific Reports*, 9(1), 2754. <https://doi.org/10.1038/s41598-019-39285-0>
- Hosseini, S. M., Alibakhshi, H., Jashni, E., Parvizian, F., Shen, J. N., Taheri, M., et al. (2020). A novel layer-by-layer heterogeneous cation exchange membrane for heavy metal ions removal from water. *Journal of Hazardous Materials*, 381, Article 120884. <https://doi.org/10.1016/j.jhazmat.2019.120884>
- Huang, R., Liu, Z., Yan, B., Li, Y., Li, H., Liu, D., ... Shi, W. (2020). Layer-by-layer assembly of high negatively charged polycarbonate membranes with robust antifouling property for microalgae harvesting. *Journal of Membrane Science*, 595, Article 117488. <https://doi.org/10.1016/j.memsci.2019.117488>
- Ifuku, S., Hori, T., Izawa, H., Morimoto, M., & Saimoto, H. (2015). Preparation of zwitterionically charged nanocrystals by surface TEMPO-mediated oxidation and partial deacetylation of α -chitin. *Carbohydrate Polymers*, 122, 1–4. <https://doi.org/10.1016/j.carbpol.2014.12.060>
- Ifuku, S., Nogi, M., Abe, K., Yoshioka, M., Morimoto, M., Saimoto, H., & Yano, H. (2009). Preparation of chitin nanofibers with a uniform width as α -chitin from crab shells. *Biomacromolecules*, 10(6), 1584–1588. <https://doi.org/10.1021/bm900163d>
- Isogai, A., Saito, T., & Fukuzumi, H. (2011). TEMPO-oxidized cellulose nanofibers. *Nanoscale*, 3(1), 71–85. <https://doi.org/10.1039/c0nr00583e>
- Kalaycioglu, G. D., & Aydogan, N. (2020). Layer-by-layer coated microcapsules with lipid nanodomains for dual-drug delivery. *Colloids and Surfaces A: Physicochemical and Engineering Aspects*, 584, Article 124037. <https://doi.org/10.1016/j.colsurfa.2019.124037>
- Kim, T., Tran, T. H., Hwang, S. Y., Park, J., Oh, D. X., & Kim, B. S. (2019). Crab-on-a-tree: All biorenewable, optical and radio frequency transparent barrier nanocoating for food packaging. *ACS Nano*, 13(4), 3796–3805. <https://doi.org/10.1021/acsnano.8b08522>
- Kiryukhin, M. V., Lau, H. H., Goh, S. H., Teh, C., Korzh, V., & Sadovoy, A. (2018). A membrane film sensor with encapsulated fluorescent dyes towards express freshness monitoring of packaged food. *Talanta*, 182, 187–192. <https://doi.org/10.1016/j.talanta.2018.01.085>
- Kumar, A., & Dixit, C. K. (2017). Methods for characterization of nanoparticles. In S. Nimesh, R. Chandra, & N. Gupta (Eds.), *Advances in Nanomedicine for the delivery of therapeutic nucleic acids* (1st ed., pp. 43–58). Duxford: Woodhead Publishing. <https://doi.org/10.1016/B978-0-08-100557-6.00003-1>
- Kumirska, J., Czerwicka, M., Kaczyński, Z., Bychowska, A., Brzozowski, K., Thöming, J., & Stepnowski, P. (2010). Application of spectroscopic methods for structural analysis of chitin and chitosan. *Marine Drugs*, 8(5), 1567–1636. <https://doi.org/10.3390/md8051567>
- Lange, J., & Wyser, Y. (2003). Recent innovations in barrier technologies for plastic packaging? A review. *Packaging Technology and Science*, 16(4), 149–158. <https://doi.org/10.1002/pts.621>
- Lanyi, F. J., Wenzke, N., Kaschta, J., & Schubert, D. W. (2020). On the determination of the enthalpy of fusion of α -crystalline isotactic polypropylene using differential scanning calorimetry, x-ray diffraction, and fourier-transform infrared spectroscopy: An old story revisited. *Advanced Engineering Materials*, 22(9), Article 1900796. <https://doi.org/10.1002/adem.201900796>
- Liu, X., Zhang, Q., Peng, B., Ren, Y., Cheng, B., Ding, C., et al. (2020). Flame retardant cellulosic fabrics via layer-by-layer self-assembly double coating with egg white protein and phytic acid. *Journal of Cleaner Production*, 243, Article 118641. <https://doi.org/10.1016/j.jclepro.2019.118641>
- Liu, Y., & Kim, H.-J. (2015). Use of attenuated total reflection fourier transform infrared (ATR FT-IR) spectroscopy in direct, nondestructive, and rapid assessment of developmental cotton fibers grown in planta and in culture. *Applied Spectroscopy*, 69(8), 1004–1010. <https://doi.org/10.1366/15-07876>
- Liu, Y., Liu, M., Yang, S., Luo, B., & Zhou, C. (2018). Liquid crystalline behaviors of chitin nanocrystals and their reinforcing effect on natural rubber. *ACS Sustainable Chemistry & Engineering*, 6(1), 325–336. <https://doi.org/10.1021/acssuschemeng.7b02586>
- Lu, P., Guo, M., Xu, Z., & Wu, M. (2018). Application of nanofibrillated cellulose on BOPP/LDPE film as oxygen barrier and antimicrobial coating based on cold plasma treatment. *Coatings*, 8(6), 207. <https://doi.org/10.3390/coatings8060207>
- Lu, Y., Sun, Q., She, X., Xia, Y., Liu, Y., Li, J., & Yang, D. (2013). Fabrication and characterisation of α -chitin nanofibers and highly transparent chitin films by pulsed ultrasonication. *Carbohydrate Polymers*, 98(2), 1497–1504. <https://doi.org/10.1016/j.carbpol.2013.07.038>
- Luo, J., Chen, W., Song, H., & Liu, J. (2020). Fabrication of hierarchical layer-by-layer membrane as the photocatalytic degradation of foulants and effective mitigation of membrane fouling for wastewater treatment. *Science of the Total Environment*, 699, Article 134398. <https://doi.org/10.1016/j.scitotenv.2019.134398>
- MacManus, L. F., Walzak, M. J., & McIntyre, N. S. (1999). Study of ultraviolet light and ozone surface modification of polypropylene. *Journal of Polymer Science Part A: Polymer Chemistry*, 37(14), 2489–2501. [https://doi.org/10.1002/\(SICI\)1099-0518\(19990715\)37:14<2489::AID-POLA23>3.0.CO;2-G](https://doi.org/10.1002/(SICI)1099-0518(19990715)37:14<2489::AID-POLA23>3.0.CO;2-G)
- Maier, C., & Calafut, T. (1998). *Polypropylene: The definitive user's guide and databook* (1st ed.) (1st ed., vol. 36). Norwich: Plastics Design Library.
- Marais, A., Uttsel, S., Gustafsson, E., & Wägberg, L. (2014). Towards a super-strainable paper using the Layer-by-Layer technique. *Carbohydrate Polymers*, 100, 218–224. <https://doi.org/10.1016/j.carbpol.2013.03.049>
- Marchessault, R. H., Morehead, F. F., & Walter, N. M. (1959). Liquid crystal systems from fibrillar polysaccharides. *Nature*, 184(4686), 632–633. <https://doi.org/10.1038/184632a0>
- Marsh, K., & Bugusu, B. (2007). Food packaging - Roles, materials, and environmental issues: Scientific status summary. *Journal of Food Science*, 72(3), R39–R55. <https://doi.org/10.1111/j.1750-3841.2007.00301.x>
- Michiels, Y., Van Puyvelde, P., & Sels, B. (2017). Barriers and chemistry in a bottle: Mechanisms in today's oxygen barriers for tomorrow's materials. *Applied Sciences*, 7(7), 665. <https://doi.org/10.3390/app7070665>
- Nair, S. S., Chen, H., Peng, Y., Huang, Y., & Yan, N. (2018). Poly(lactic acid) biocomposites reinforced with nanocellulose fibrils with high lignin content for improved mechanical, thermal, and barrier properties. *ACS Sustainable Chemistry and Engineering*, 6(8), 10058–10068. <https://doi.org/10.1021/acssuschemeng.8b01405>
- Nakaya, M., Uedono, A., & Hotta, A. (2015). Recent progress in gas barrier thin film coatings on PET bottles in food and beverage applications. *Coatings*, 5(4), 987–1001. <https://doi.org/10.3390/coatings5040987>
- Nguyen, H.-L., Hanif, Z., Park, S.-A., Choi, B., Tran, T., Hwang, D., et al. (2018). Sustainable boron nitride nanosheet-reinforced cellulose nanofiber composite film with oxygen barrier without the cost of color and cytotoxicity. *Polymers*, 10(5), 501. <https://doi.org/10.3390/polym10050501>
- Nguyen, H.-L., Jo, Y., Cha, M., Cha, Y., Yoon, D., Sanandiya, N., et al. (2016). Mussel-inspired anisotropic nanocellulose and silver nanoparticle composite with improved mechanical properties, electrical conductivity and antibacterial activity. *Polymers*, 8(3), 102. <https://doi.org/10.3390/polym8030102>

- Ni, Y. Q., Ding, S., Han, B., & Wang, H. (2019). Layer-by-layer assembly of polyelectrolytes-wrapped multi-walled carbon nanotubes on long period fiber grating sensors. *Sensors and Actuators, B: Chemical*, 301, Article 127120. <https://doi.org/10.1016/j.snb.2019.127120>
- Nikolov, S., Petrov, M., Lymerakis, L., Friák, M., Sachs, C., Fabritius, H. O., et al. (2010). Revealing the design principles of high-performance biological composites using Ab initio and multiscale simulations: The example of lobster cuticle. *Advanced Materials*, 22(4), 519–526. <https://doi.org/10.1002/adma.200902019>
- Ogawa, Y., Hori, R., Kim, U. J., & Wada, M. (2011). Elastic modulus in the crystalline region and the thermal expansion coefficients of α -chitin determined using synchrotron radiated X-ray diffraction. *Carbohydrate Polymers*, 83(3), 1213–1217. <https://doi.org/10.1016/j.carbpol.2010.09.025>
- Oytun, F., & Basarir, F. (2019). Spin-assisted layer-by-layer assembled oppositely charged reduced graphene oxide films. *Materials Letters*, 257, Article 126756. <https://doi.org/10.1016/j.matlet.2019.126756>
- Ozcalik, O., & Tihminlioglu, F. (2013). Barrier properties of corn zein nanocomposite coated polypropylene films for food packaging applications. *Journal of Food Engineering*, 114(4), 505–513. <https://doi.org/10.1016/j.jfoodeng.2012.09.005>
- Parameswaranpillai, J., Joseph, G., Shinu, K. P., Sreejesh, P. R., Jose, S., Salim, N. V., & Hameed, N. (2015). The role of SEBS in tailoring the interface between the polymer matrix and exfoliated graphene nanoplatelets in hybrid composites. *Materials Chemistry and Physics*, 163, 182–189. <https://doi.org/10.1016/j.matchemphys.2015.07.028>
- Park, S.-A., Jeon, H., Kim, H., Shin, S.-H., Choy, S., Hwang, D. S., et al. (2019). Sustainable and recyclable super engineering thermoplastic from bio-renewable monomer. *Nature Communications*, 10(1), 2601. <https://doi.org/10.1038/s41467-019-10582-6>
- Prata, J. C., Silva, A. L. P., Walker, T. R., Duarte, A. C., & Rocha-Santos, T. (2020). COVID-19 pandemic repercussions on the use and management of plastics. *Environmental Science & Technology*, 54(13), 7760–7765. <https://doi.org/10.1021/acs.est.0c02178>
- Priolo, M. A., Gamboa, D., Holder, K. M., & Grunlan, J. C. (2010). Super gas barrier of transparent polymer-clay multilayer ultrathin films. *Nano Letters*, 10(12), 4970–4974. <https://doi.org/10.1021/nl103047k>
- Priolo, M. A., Holder, K. M., Gamboa, D., & Grunlan, J. C. (2011). Influence of clay concentration on the gas barrier of clay-polymer nanobrick wall thin film assemblies. *Langmuir*, 27(19), 12106–12114. <https://doi.org/10.1021/la201584r>
- Priolo, M. A., Holder, K. M., Guin, T., & Grunlan, J. C. (2015). Recent advances in gas barrier thin films via layer-by-layer assembly of polymers and platelets. *Macromolecular Rapid Communications*, 36(10), 866–879. <https://doi.org/10.1002/marc.201500055>
- Qi, Z.-D., Saito, T., Fan, Y., & Isogai, A. (2012). Multifunctional coating films by layer-by-layer deposition of cellulose and chitin nanofibrils. *Biomacromolecules*, 13(2), 553–558. <https://doi.org/10.1021/bm201659b>
- Qiu, X., Kundu, C. K., Li, Z., Li, X., & Zhang, Z. (2019). Layer-by-layer-assembled flame-retardant coatings from polydopamine-induced in situ functionalized and reduced graphene oxide. *Journal of Materials Science*, 54(21), 13848–13862. <https://doi.org/10.1007/s10853-019-03879-w>
- Reid, M. S., Villalobos, M., & Cranston, E. D. (2017). Benchmarking cellulose nanocrystals: From the laboratory to industrial production. *Langmuir*, 33(7), 1583–1598. <https://doi.org/10.1021/acs.langmuir.6b03765>
- Revol, J.-F., & Marchessault, R. H. (1993). In vitro chiral nematic ordering of chitin crystallites. *International Journal of Biological Macromolecules*, 15(6), 329–335. [https://doi.org/10.1016/0141-8130\(93\)90049-R](https://doi.org/10.1016/0141-8130(93)90049-R)
- Richardson, J. J., Björnalm, M., & Caruso, F. (2015). Technology-driven layer-by-layer assembly of nanofilms. *Science*, 348(6233), aaa2491–aaa2491. doi:<https://doi.org/10.1126/science.aaa2491>
- Richardson, J. J., Cui, J., Björnalm, M., Braunger, J. A., Ejima, H., & Caruso, F. (2016). Innovation in layer-by-layer assembly. *Chemical Reviews*, 116(23), 14828–14867. <https://doi.org/10.1021/acs.chemrev.6b00627>
- Sahariah, P., & Måsson, M. (2017). Antimicrobial chitosan and chitosan derivatives: A review of the structure–activity relationship. *Biomacromolecules*, 18(11), 3846–3868. <https://doi.org/10.1021/acs.biomac.7b01058>
- Saito, T., Kimura, S., Nishiyama, Y., & Isogai, A. (2007). Cellulose nanofibers prepared by TEMPO-mediated oxidation of native cellulose. *Biomacromolecules*, 8(8), 2485–2491. <https://doi.org/10.1021/bm0703970>
- Sangroniz, A., Zhu, J.-B., Tang, X., Etxeberria, A., Chen, E. Y.-X., & Sardon, H. (2019). Packaging materials with desired mechanical and barrier properties and full chemical recyclability. *Nature Communications*, 10(1), 3559. <https://doi.org/10.1038/s41467-019-11525-x>
- Sato, K., Tominaga, Y., & Imai, Y. (2020). Nanocelluloses and related materials applicable in thermal management of electronic devices: A review. *Nanomaterials*, 10(3), 448. <https://doi.org/10.3390/nano10030448>
- Schneiderman, D. K., & Hillmyer, M. A. (2017). 50th anniversary perspective: There is a great future in sustainable polymers. *Macromolecules*, 50(10), 3733–3749. <https://doi.org/10.1021/acs.macromol.7b00293>
- Schramm, C. (2020). High temperature ATR-FTIR characterization of the interaction of polycarboxylic acids and organotralkoxysilanes with cellulosic material. *Spectrochimica Acta Part A: Molecular and Biomolecular Spectroscopy*, 243, Article 118815. <https://doi.org/10.1016/j.saa.2020.118815>
- Segal, L., Creely, J. J., Martin, A. E., & Conrad, C. M. (1959). An empirical method for estimating the degree of crystallinity of native cellulose using the x-ray diffractometer. *Textile Research Journal*, 29(10), 786–794. <https://doi.org/10.1177/004051755902901003>
- Song, Y., Tzeng, P., & Grunlan, J. C. (2016). Super oxygen and improved water vapor barrier of polypropylene film with polyelectrolyte multilayer nanocoatings. *Macromolecular Rapid Communications*, 37(12), 963–968. <https://doi.org/10.1002/marc.201600140>
- Stocchetti, G. (2012). Technology that bridges the gap. *Packaging Films*, 3(1), 16–18.
- Struller, C. F., Kelly, P. J., & Copeland, N. J. (2014). Aluminum oxide barrier coatings on polymer films for food packaging applications. *Surface and Coatings Technology*, 241, 130–137. <https://doi.org/10.1016/j.surfcoat.2013.08.011>
- Sun, J., Du, Y., Ma, J., Li, Y., Wang, L., Lu, Y., et al. (2019). Transparent bionanocomposite films based on konjac glucomannan, chitosan, and TEMPO-oxidized chitin nanocrystals with enhanced mechanical and barrier properties. *International Journal of Biological Macromolecules*, 138, 866–873. <https://doi.org/10.1016/j.ijbiomac.2019.07.170>
- Tang, Z., Li, W., Lin, X., Xiao, H., Miao, Q., Huang, L., et al. (2017). TEMPO-oxidized cellulose with high degree of oxidation. *Polymers*, 9(9), 421. <https://doi.org/10.3390/polym9090421>
- Tian, W., VahidMohammadi, A., Wang, Z., Ouyang, L., Beidaghi, M., & Hamed, M. M. (2019). Layer-by-layer self-assembly of pillared two-dimensional multilayers. *Nature Communications*, 10(1), 2558. <https://doi.org/10.1038/s41467-019-10631-0>
- Tran, C. T. H., Craggs, M., Smith, L. M., Stanley, K., Kondyurin, A., Bilek, M. M., & McKenzie, D. R. (2016). Covalent linker-free immobilization of conjugatable oligonucleotides on polypropylene surfaces. *RSC Advances*, 6(86), 83328–83336. <https://doi.org/10.1039/c6ra16034d>
- Tran, T. H., Nguyen, H. L., Hwang, D. S., Lee, J. Y., Cha, H. G., Koo, J. M., et al. (2019). Five different chitin nanomaterials from identical source with different advantageous functions and performances. *Carbohydrate Polymers*, 205, 392–400. <https://doi.org/10.1016/j.carbpol.2018.10.089>
- Vahedikia, N., Garavand, F., Tajeddin, B., Cacciotti, I., Jafari, S. M., Omid, T., & Zahedi, Z. (2019). Biodegradable zein film composites reinforced with chitosan nanoparticles and cinnamon essential oil: Physical, mechanical, structural and antimicrobial attributes. *Colloids and Surfaces B: Biointerfaces*, 177, 25–32. <https://doi.org/10.1016/j.colsurfb.2019.01.045>
- Vasile, C. (2018). Polymeric nanocomposites and nanocoatings for food packaging: A review. *Materials*, 11(10), 1834. <https://doi.org/10.3390/ma11101834>
- Wågberg, L., Decher, G., Norgren, M., Lindström, T., Ankerfors, M., & Axnäs, K. (2008). The build-up of polyelectrolyte multilayers of microfibrillated cellulose and cationic polyelectrolytes. *Langmuir*, 24(3), 784–795. <https://doi.org/10.1021/la702481v>
- Walzak, M. J., Flynn, S., Foerch, R., Hill, J. M., Karbaszewski, E., Lin, A., & Strobel, M. (1995). UV and ozone treatment of polypropylene and poly(ethylene terephthalate). *Journal of Adhesion Science and Technology*, 9(9), 1229–1248. <https://doi.org/10.1163/156856195X01012>
- Wang, H., Qian, C., & Roman, M. (2011). Effects of pH and salt concentration on the formation and properties of chitosan–cellulose nanocrystal polyelectrolyte–macroion complexes. *Biomacromolecules*, 12(10), 3708–3714. <https://doi.org/10.1021/bm2009685>
- Wang, J., Kasuya, K., Koga, H., Nogi, M., & Uetani, K. (2021). Thermal conductivity analysis of chitin and deacetylated-chitin nanofiber films under dry conditions. *Nanomaterials*, 11(3), 658. <https://doi.org/10.3390/nano11030658>
- Wang, J., Li, Z., Wang, Y., Li, Q., Chen, L., Shi, H., & Hao, J. (2020). Controllable layer-by-layer assembly based on brucite and alginates with the assistance of spray drying and flame retardancy influenced by gradients of alginates. *Journal of Applied Polymer Science*, 137(1), 47570. <https://doi.org/10.1002/app.47570>
- Wang, J., Gardner, D. J., Stark, N. M., Bousfield, D. W., Tajvidi, M., & Cai, Z. (2018). Moisture and oxygen barrier properties of cellulose nanomaterial-based films. *ACS Sustainable Chemistry and Engineering*, 6(1), 49–70. <https://doi.org/10.1021/acsschemeng.7b03523>
- Wang, Y., Kim, J. H., Choo, K. H., Lee, Y. S., & Lee, C. H. (2000). Hydrophilic modification of polypropylene microfiltration membranes by ozone-induced graft polymerization. *Journal of Membrane Science*, 169(2), 269–276. [https://doi.org/10.1016/S0376-7388\(99\)00345-2](https://doi.org/10.1016/S0376-7388(99)00345-2)
- Yagoub, H., Ma, S., Yang, S., & Xu, J. (2014). Preparation and characterisation of cellulose nanocrystals thin films utilising layer-by-layer deposition. *Materials Research Innovations*, 18(sup4), S4–821–S4–824. doi:<https://doi.org/10.1179/1432891714Z.000000000801>
- Yan, N., & Chen, X. (2015). Sustainability: Don't waste seafood waste. *Nature*, 524(7564), 155–157. <https://doi.org/10.1038/524155a>
- Yang, Y.-H., Haile, M., Park, Y. T., Malek, F. A., & Grunlan, J. C. (2011). Super gas barrier of all-polymer multilayer thin films. *Macromolecules*, 44(6), 1450–1459. <https://doi.org/10.1021/ma1026127>
- Yu, J., Ruengkajorn, K., Crivoi, D. G., Chen, C., Buffet, J. C., & O'Hare, D. (2019). High gas barrier coating using non-toxic nanosheet dispersions for flexible food packaging film. *Nature Communications*, 10(1), 2398. <https://doi.org/10.1038/s41467-019-10362-2>
- Zajac, A., Hanuza, J., Wandas, M., & Dymińska, L. (2015). Determination of N-acetylation degree in chitosan using Raman spectroscopy. *Spectrochimica Acta Part A: Molecular and Biomolecular Spectroscopy*, 134, 114–120. <https://doi.org/10.1016/j.saa.2014.06.071>
- Zhang, X., & Rolandi, M. (2017). Engineering strategies for chitin nanofibers. *Journal of Materials Chemistry B*, 5(14), 2547–2559. <https://doi.org/10.1039/C6TB03324E>
- Zimmermann, T., Pöhler, E., & Geiger, T. (2004). Cellulose fibrils for polymer reinforcement. *Advanced Engineering Materials*, 6(9), 754–761. <https://doi.org/10.1002/adem.200400097>